Frequency-specific neural signatures of perceptual content and perceptual stability

Richard Hardstone[1], Matthew Flounders[1], Michael Zhu[1], Biyu J. He[1,2,3,4*]

[1] Neuroscience Institute, New York University Grossman School of Medicine, New York, NY10016, USA
[2] Department of Neurology, New York University Grossman School of Medicine, New York, NY10016, USA
[3] Department of Neuroscience and Physiology, New York University Grossman School of Medicine, New York, NY10016, USA
[4] Department of Radiology, New York University Grossman School of Medicine, New York, NY10016, USA
*Email: biyu.he@nyulangone.org

ABSTRACT

In the natural environment, we often form stable perceptual experiences from ambiguous and fleeting sensory inputs. Which neural activity underlies the content of perception and which neural activity supports perceptual stability remains an open question. We used a bistable perception paradigm involving ambiguous images to behaviorally dissociate perceptual content from perceptual stability, and magnetoencephalography (MEG) to measure whole-brain neural dynamics in humans. Combining multivariate decoding and neural state-space analyses, we found frequency band-specific neural signatures that underlie the content of perception and promote perceptual stability, respectively. Across different types of images, non-oscillatory neural activity in the slow cortical potential (SCP, <5 Hz) range supported the content of perception. Perceptual stability was additionally influenced by the amplitude of alpha and beta oscillations. In addition, neural activity underlying perceptual memory, which supports perceptual stability when sensory input is temporally removed from view, also encodes elapsed time. Together, these results reveal distinct neural mechanisms that support the content vs. stability of visual perception.

INTRODUCTION

How vivid visual perceptual experiences are generated by the brain remains a central question in neuroscience. There are two critical functions that the visual perceptual system is able to accomplish: the first is to generate the specific content of perceptual experience (such as seeing a predator); the second is to maintain a stable perceptual experience despite noisy and unstable retinal input due to constant head and eye movements and complexities of the natural environment involving occlusion, shading, and dynamic changes of sensory input (e.g., the predator is camouflaged and hidden in the bush). Here, we investigate neural mechanisms giving rise to specific perceptual content and supporting perceptual stability in the human brain.

Motivated by several strands of previous work, we hypothesized that there might be different components of electrophysiological neural activities that support perceptual content and perceptual stability, respectively. First, previous studies using multivariate analysis to decode perceptual content based on electroencephalography/magnetoencephalography (EEG/MEG) activity have typically reported greater successes when the decoder's input was raw filtered field potentials in the relatively low (<30 Hz) frequency range [e.g., (Carlson et al., 2013; Salti et al., 2015; King et al., 2016)]. Further, studies using frequency band-specific analysis have shown that the ability to decode perceptual content is contributed most by the slow cortical potential (SCP, <5 Hz) frequency range (Baria et al., 2017; Flounders et al., 2019). This is consistent with the 1/f distribution of EEG/MEG power spectrum suggesting that the SCP band contributes most to the power in the ERP/ERF frequency range (He et al., 2010; He, 2014; Donoghue et al., 2020).

Second, a line of work focused on brain oscillations has shown that moment-to-moment fluctuations of alpha oscillation amplitude in sensory cortices modulate local cortical excitability in a manner that transcends specific stimulus/perceptual contents (Samaha et al., 2020). In addition, alpha and beta oscillations can carry top-down feedback influences (van Kerkoerle et al., 2014; Michalareas et al., 2016), and top-down feedback may facilitate resolving perceptual ambiguity by carrying information consistent with prior knowledge (Cavanagh, 1991; Yuille and Kersten, 2006). We therefore hypothesized that there might exist a frequency-band separation between neural activity supporting perceptual content and neural activity supporting perceptual stability, with the former residing in the non-oscillatory activity in the SCP range, and the latter predominantly residing in oscillatory activity in the alpha/beta range.

To test this hypothesis, we recorded whole-head MEG while participants performed a bistable visual perception task involving two different ambiguous figures (Necker cube and Rubin face-vase illusion). Data from these two images were separately analyzed, providing a within-study reproducibility and generalizability check. In two different conditions, the images were either continuously presented (*Ambiguous* condition, Figure 1A) or intermittently presented (*Discontinuous* condition, Figure 1E). The *Ambiguous* condition allowed us to dissociate perceptual content (perceiving one or the other interpretation) from perceptual stability (how long a percept lasts). The *Discontinuous* condition allowed us to investigate the neural underpinnings of perceptual memory: previous research has shown that perceptual alternations slow down during intermittent presentation and that a perceptual memory trace exists in the intervening blank periods such that the recently experienced percept is likely reinstated when the image reappears (Orbach et al., 1966; Leopold et al., 2002; Pearson and Brascamp, 2008). This phenomenon provides a window into neural mechanisms supporting perceptual stability when sensory input is both ambiguous and fleeting, as often is the case in natural vision. Finally, to test the generalizability of the identified neural correlate of perceptual content, participants additionally performed a task in which modified versions of the Necker cube and Rubin face-vase images with ambiguity removed (Wang et al., 2013) were presented and perceptual content varied with the actual physical stimulus (*Unambiguous* condition, Figure 1C).

To test our hypothesis, we combined multivariate decoding with an innovative multivariate regression approach which allowed us to identify separate neural subspaces relevant to the encoding of different types of behavioral information that are simultaneously present in the same task (Mante et al., 2013)—specifically, perceptual content and perceptual switching dynamics in the present task. Across two different task conditions with different levels of stimulus ambiguity (*Ambiguous* and *Unambiguous*), we found that non-oscillatory neural activity in the SCP range, but not alpha or beta oscillations, encoded perceptual content. Furthermore, across both *Ambiguous* and *Discontinuous* conditions, we found that the fluctuations of alpha and beta amplitudes modulated perceptual stability and perceptual memory. Interestingly, we also found that SCP modulated perceptual stability, although with less spatial consistency across subjects than alpha and beta oscillations. These results reveal an intriguing frequency-domain separation of neural activity encoding perceptual content and that supporting perceptual stability.

RESULTS

Task paradigm and behavioral results

We recorded eighteen subjects with whole-head MEG (CTF, 272 functional axial gradiometers) performing three conditions of a visual perception task involving two commonly studied ambiguous figures (Necker cube and Rubin face-vase illusion). The first condition consists of the classic bistable perception task (*Ambiguous,* Figure 1A), in which subjects viewed ambiguous images for 60 seconds at a time and used button presses to indicate their spontaneous perceptual switches (with three buttons corresponding to two of the possible percepts and an 'unsure' option). In the second condition (*Unambiguous,* Figure 1C), subjects viewed modified versions of these images for 5 seconds at a time, which enhance one of the possible interpretations and largely abolish perceptual switching (Wang et al., 2013); subjects indicated their percepts in a similar fashion as before. In the final condition (*Discontinuous,* Figure 1E), each ambiguous figure was presented repeatedly with interleaving blank periods, allowing us to investigate neural underpinnings of perceptual memory during the blank periods (Leopold et al., 2002; Pearson and Brascamp, 2008); subjects indicated their percepts whenever the image was in view.

During the *Ambiguous* condition (Figure 1A,B) perceptual switching occurred, with group-level results showing that each of the possible percepts was perceived (on average > 25% of the time), and that subjects were rarely unsure of which percept they were experiencing (< 10% occurrence, these time periods were removed from further analyses). Modifying the images to be unambiguous (Figure 1C,D) was successful, as evidenced by subjects having on average > 80% valid trials (defined as trials with only one button press indicating the intended percept). In the *Discontinuous* condition we found an increased likelihood that perception remained stable across the blank period for the Necker cube (one-tailed Wilcoxon Sign-Rank(17)=116.5, p=0.031) but not for the Rubin face-vase image (one-tailed Wilcoxon Sign-Rank(17)=71.5, p=0.736).

Together, these behavioral results demonstrate the classic bistable perception phenomenon in the *Ambiguous* condition, successful disambiguation of the images in the *Unambiguous* condition, and a means to investigate perceptual memory by contrasting stable and unstable blank periods in the *Discontinuous* condition. Importantly, the use of two different ambiguous figures in all three conditions allowed us to test whether the neural findings are reproducible and generalizable across the specific stimulus characteristics. Here, taking advantage of the large-scale neural dynamics recorded by whole-head MEG, we aimed to dissociate dynamical neural activity underlying perceptual content and supporting perceptual stability, respectively.

Perceptual content can be decoded from SCP but not amplitude of band-limited oscillations

In the classic bistable perception task, perceptual content experienced by the subject continuously alternates between two possible outcomes while the sensory input stays constant. This allows the investigation of the neural correlates of the content of conscious perception while controlling for low-level sensory processing. To this end, we applied time-resolved multivariate decoding to whole-brain MEG data (for details, see *Methods*). We tested three components of neural field potentials — slow-cortical potential (SCP, < 5 Hz), alpha-band amplitude (amplitude envelope of 8-13 Hz filtered data) and beta-band amplitude (amplitude envelope of 13-30 Hz filtered data) — in their ability to distinguish between the two percepts that are alternatively experienced for each ambiguous figure. The SCP activity corresponds to the low-frequency component of the broadband, non-oscillatory (i.e., aperiodic) activity (He et al., 2010; He, 2014), while the alpha and beta bands have prominent oscillatory activity (Figure 1—figure supplement 1A-B). After extracting the relevant neural feature, perceptual content decoding was performed using a four-fold cross-validated linear support vector machine, with significance determined using cluster-based permutation testing that corrects for multiple comparisons across time.

To investigate neural activity underlying specific perceptual content, we selected time periods ('sub-trials') that were preceded and followed by button presses for two different percepts (i.e., excluding periods preceded or followed by unsure presses, or at the beginning or end of the image presentation) and sorted them into two groups. Thus, each sub-trial begins with a button press indicating the relevant percept and ends with a button press that indicates a switch to the opposite percept. These sub-trials were of different lengths (Figure 1—figure supplement 1C-D), as percept duration is highly variable during spontaneous bistable perception—a topic we will address in the following section. To decode perceptual content, we then subsampled each sub-trial by taking 100 equally spaced time points from the beginning to the end of that sub-trial (henceforth referred to as percentile of a percept). This way, we tested whether a decoder trained using neural features recorded at the beginning (/middle/end) of a sub-trial generalized to the beginning (/middle/end) of other sub-trials, even if they were of different lengths (Figure 2A).

Decoding accuracies over the course of a percept for the three different neural features are shown in Figure 2C, left column. Significant decoding of perceptual content is found for SCP, but not alpha or beta amplitude (except for a very small temporal cluster for the face-vase image), and SCP shows significantly stronger decoding than alpha or beta amplitude (Figure 2—figure supplement 1) suggesting that the currently experienced percept is most strongly encoded in SCP activity. These findings are consistent with previous results using other visual perceptual tasks (Baria et al., 2017; Flounders et al., 2019). To shed light on whether the neural representation of the percept stays stable over the duration of the percept or changes constantly over time, we tested the temporal generalization of the decoder, whereby decoders trained at each timepoint are tested at all other timepoints (King and Dehaene, 2014). We observed broad decoder temporal generalization in the SCP band for both the Necker cube and Rubin face-vase illusion (Figure 2C, right column), especially from 20^{th} to 80^{th} percentile of the percept duration. This suggests that neural representation underlying perceptual content, except at the very beginning and end of a percept, is relatively stable over time regardless of percept duration, and localizes to the SCP band in the frequency domain.

We next tested whether a similar pattern of findings exists when stimulus ambiguity is removed, by decoding perceptual content using data from the *Unambiguous* condition. To this end, we selected valid trials (wherein the subject only had one button press indicating the intended percept), which account for the vast majority of all trials (Figure 1D), and constructed decoders to distinguish between the two different perceptual contents which coincided with different image inputs (i.e., decoding between the two versions of face-vase image, and between the two versions of cube image, Figure 2B). Similar to the *Ambiguous* condition, significant perceptual content decoding was obtained using SCP activity, but not alpha or beta amplitude (except for one small temporal cluster

at image onset for alpha amplitude, face-vase image) (Figure 2D, left column) and decoding was stronger in the SCP band (Figure 2—figure supplement 1). Decoding accuracy in the SCP band was highest in the first second after image onset and then drops to a lower level (likely due to neural adaptation). The higher decoding accuracy in the *Unambiguous* condition as compared to the *Ambiguous* condition is likely due to the differences in sensory input that coincides with different perceptual contents, as well as consistent timing across all trials (all image presentations last 5 seconds, as opposed to variable percept durations in the *Ambiguous* condition). Lastly, as in the *Ambiguous* condition, the SCP decoder of perceptual content generalized well across time in the *Unambiguous* condition (Figure 2D, right column), suggesting that the underlying neural code is stable over time after the very initial image onset-related activity.

Together, these results show that perceptual content information is decodable from SCP activity, but not from the amplitude of alpha or beta oscillations, regardless of whether sensory input is ambiguous or not. In the next section we investigate neural processes controlling the stability of a percept as compared to the neural processes underlying the content of that percept.

Defining a behaviorally relevant neural subspace

To simultaneously extract neural activity relevant to different behavioral metrics—here, the content of perception and the dynamics of perceptual switching—we adapted a multivariate analysis approach recently developed in animal neurophysiology ('state space analysis') (Sussillo, 2014). In this framework, multivariate neural activity (across neurons or sensors) at each time point corresponds to a specific location in the neural state space, where each dimension is a neuron/sensor. Because different neurons/sensors are highly correlated and not all are informative for the behavior of interest, dimensionality reduction methods (such as principal component analysis, PCA) are typically applied to identify a low-dimensional subspace capturing the majority of the variance in the data and/or most relevant to the behavior in question (Briggman et al., 2005; Churchland et al., 2012; Stokes et al., 2013; Baria et al., 2017). Here, following earlier studies (Mante et al., 2013; Kayser et al., 2016), we identify the neural subspace most relevant to a particular behavioral metric by conducting a multilinear regression using orthogonal, task-related axes that capture perceptual content and perceptual switching dynamics, as described in detail below. Importantly, unlike the decoding approach employed in the earlier analysis, where a different decoder is trained for each time point within a trial and decoder weights are sometimes difficult to interpret (Haufe et al., 2014), the state space analysis aims to identify a neural subspace that is unchanging across time, wherein the trajectory of neural activity informs about changes in behavior across time.

For both the *Ambiguous* and *Discontinuous* conditions, we defined a set of behavioral axes capturing both perceptual content and perceptual switching dynamics (Figure 3A). For the *Ambiguous* condition, these consisted of a *Type* Axis, which was a binary (0 or 1) variable indicating the current perceptual content; a *Duration* Axis, indicating the overall duration of the current percept; a *Switch* Axis, indicating the temporal distance to a reported perceptual switch (i.e., button press); and, finally, a *Direction* Axis, a binary variable indicating whether the current percept is stabilizing or destabilizing (operationalized as the first half vs. second half of a percept). Both the Switch and Duration axes had values normalized to the range of [0, 1], such that for the *Switch* axis, time points corresponding to button presses are 0 and time points furthest away from button presses within each percept are 1; for the *Duration* axis, the shorted and longest percept durations for a particular subject are coded as 0 and 1, respectively. Thus, the *Switch*, *Duration*, and *Direction* axes together capture different aspects of the perceptual switching dynamic, while the *Type* axis captures the specific perceptual content.

For the *Discontinuous* condition, because we are interested in neural activity underlying the perceptual memory trace, only blank periods were analyzed. Two behavioral axes were defined to capture the content of perception: *Pre* and *Post*, which are binary variables indicating the perceptual content before and after the blank period, respectively. Two behavioral axes were defined to capture the dynamics of perceptual memory: a *Memory* axis, which is a binary variable indicating whether a perceptual memory trace is present or absent (defined by whether the reported perceptual content before and after the blank period is the same); and a *Blank* axis, which is a linearly ramping variable between 0 and 1 from the beginning to the end of each blank period, indicating how long the perceptual memory trace, if present, has last since image offset.

To extract the neural subspace most relevant to each behavioral metric, half of the data were used as a training set and a multi-linear regression model was fit for each sensor (Figure 3B). The β weights from the regression model provide an estimate of the relative contributions of the activity of that sensor to each of the different behavioral metrics. The set of weights across sensors for a particular behavioral metric thus defines the identified neural subspace. The held-out test data is then projected into that subspace (Figure 3C), which provides a prediction of the value of that behavioral metric at each time point, solely based on the MEG activity. Comparing the actual and predicted behavior (Figure 3D) yields a cross-validated estimate of how much information the identified neural subspace has about that aspect of behavior.

Lastly, the set of β weights (with size equal to the number of MEG sensors) for each behavioral metric can also be inspected for consistency at the group level (topography in Figure 3B) to determine whether neural activity from a particular sensor significantly contributes to a particular behavioral metric. In sum, this state space analysis allows us to simultaneously identify neural underpinnings of multiple aspects of behavior at once.

Role of neural oscillations in perceptual switching dynamics during bistable perception

We first applied the state space analysis to data from the *Ambiguous* condition. For perceptual content ('Type' axis), we found that the neural subspace identified using the SCP activity allows robust prediction of moment-to-moment perceptual content experienced by the subject for the face-vase image (Figure 4—figure supplement 1B, 'Type' column), with highly consistent sensor-level weights across subjects (Figure 4—figure supplement 1A, 'Type' column). Interestingly, the results did not reach significance for the cube image, consistent with weaker perceptual content decoding for the cube than face-vase image (Figure 2A) and potentially due to the decoder being re-trained at each time point whereas the subspace is fixed across timepoints. Using amplitude of alpha or beta oscillations, we could not achieve significant prediction of perceptual content (except for a small temporal cluster for beta amplitude, cube image) (Figure 4—figure supplement 1B, 'Type' column) and there was no consistent weights across subjects (Figure 4—figure supplement 1A, 'Type' column). Together, these results reinforce the impression from the decoding results showing that perceptual content information largely localizes to the SCP band, manifesting as moment-to-moment changes in large-scale SCP activity.

Focusing on the 'Duration' axis, which captures variability in the percept durations, we found consistent group-level β weights in occipital cortex for alpha and beta amplitude, whereby stronger neural oscillations were associated with longer lasting percepts (Figure 4A, left; reproduced in Figure 4—figure supplement 1A, 'Duration' column). The 'Duration' neural subspace extracted from alpha and beta amplitudes contained significant predictive information for percept durations in the left-out test data set, as evidenced by highly significant correlations between the actual percept duration and predicted percept duration according to neural data collected at different time points during a percept (Figure 4A, right, showing trial-by-trial correlation; Figure 4—figure supplement 1B, 'Duration' column, showing predicted percept durations for trials with long vs. short actual percept

durations). These results also show that neural activity related to perceptual stability is relatively persistent across time, evident from the beginning to the end of a percept. For SCP activity, significant predictive information over time was found for both images (Figure 4—figure supplement 1B, 'Duration' column); however, there was little consistency between β weights across subjects (Figure 4—figure supplement 1A, 'Duration' column), or between the group-level β weight maps for the two images (cosine similarity, N=272 sensors, Cos θ = 0.08, p=0.37 assessed by a permutation test). By contrast, the group-level β weight maps for the 'Duration' axis are highly correlated between the two images for alpha amplitude (Cos θ = 0.83, p=0.02) and beta amplitude (Cos θ = 0.82, p=0.02). Therefore, we conclude that information about perceptual stability, as captured by percept duration, is primarily carried by the amplitude of alpha- and beta-band activity. Although this information also exists in the SCP band, it is encoded in a less consistent manner across subjects and across different image inputs.

For the 'Switch' and 'Direction' axes, we found that all three neural features were significantly predictive of behavior (Figure 4—figure supplement 1B, 'Switch' and 'Direction' columns), suggesting that the neural representation of these processes is distributed across multiple frequency bands. For the 'Direction' axis, group-level β weight maps for SCP and beta amplitude show significant sensors lateralized over the left hemisphere whose spatial distribution could be related to the button press response (carried out using the right hand). For the 'Switch' axis, the SCP-band β weight maps are consistent with a dipole in the midline region corresponding to a potential source in the supplementary motor area; alpha/beta amplitudes have positive β weights suggesting that the amplitudes decrease around the time of the perceptual switch, consistent with earlier findings (de Jong et al., 2016). Together, these findings provide a methodological validation of the present analysis approach; however, given the potential motor contribution to the results obtained from the 'Switch' and 'Direction' behavioral axes, we do not emphasize these findings henceforth.

Role of neural oscillations in maintaining perceptual memory

Finally, we applied the state space analysis to data from the *Discontinuous* condition, focusing on the blank periods (6-sec each) between repeated image presentations (Figure 1E). For perceptual content reported before and after each blank period ('Pre' and 'Post' axes), we only found small temporal clusters of significant prediction in the test data set for beta amplitude-defined neural subspace in the case of cube image (Figure 4—figure supplement 2B, 'Pre' and 'Post' columns). Overall, the information contained in neural activity during blank periods about perceptual content experienced earlier or later is weak, which is not surprising, given that there is no active perception related to the cube or face-vase image per se during this period.

However, all three neural features carried significant information about how far into the blank period the timepoint was (i.e., the temporal distance to previous image offset), suggesting a strong timing mechanism distributed across frequency bands. This is evident in the ability of the neural subspaces to predict timing information in the left-out test data set (Figure 4—figure supplement 2B, 'Blank' column), as well as consistent sensor-level β weight topography across subjects (Figure 4—figure supplement 2A, 'Blank' column). The SCP topography shows a midline dipole, and the alpha/beta topographies show widespread sensors whose oscillatory amplitudes decrease as time passes. Because the blank periods have a constant duration (6 sec) before the next image onset, these results are consistent with previous reports of a contingent negative variation potential (CNV, an SCP activity with generators in the anterior cingulate cortex) and alpha amplitude decreases being neural correlates of temporal anticipation (Nobre and van Ede, 2018).

The most informative behavioral metric for the *Discontinuous* condition is the 'Memory' axis as it indicates the presence or absence of a perceptual memory trace (Figure 3A). Here we found significant temporal clusters of prediction in the test data set using alpha and beta amplitudes, but

not SCP activity (which only showed small temporal clusters for the Cube image) (Figure 4—figure supplement 2B, 'Memory' column; alpha and beta results reproduced in Figure 4B). The consistency of the group-level β weights across images was also stronger for alpha (cos θ = 0.65, p=0.08) and beta amplitude (cos θ = 0.75, p=0.10) than for SCP activity (cos θ = -0.11, p=0.71), although the consistency did not reach significance in any of the neural features. Interestingly, the group-level β weight vectors are highly correlated between the Memory axis and the Blank axis for alpha and beta amplitude (alpha amplitude: Face-vase, cos θ = 0.84, p<0.01; Cube: cos θ = 0.82, p=0.01; beta amplitude: Face-vase, cos θ = 0.83, p=0.02, Cube: cos θ = 0.86, p<0.01), suggesting a strong timing component to the memory trace. The negative β weights for the oscillation amplitudes (Figure 4B, left) show that alpha and beta oscillations are weaker when there is a perceptual memory trace.

Interestingly, the encoding of perceptual memory during the blank periods occurs first in beta activity (at ~0.5–1.5 sec after blank onset), followed by alpha activity (at ~1.5–3 sec), and is not significant in either frequency band during the latter half of the blank period (3–6 sec) (Fig. 4B and Figure 4—figure supplement 2). This transient encoding of perceptual memory in neural dynamics is consistent with a recent EEG study using a similar paradigm (Zhu et al., 2022). Speculatively, after the transient encoding in beta and alpha activity, perceptual memory trace might be maintained in short-term synaptic plasticity within the network in an "activity-silent" state without measurable signatures in active neural dynamics (Mongillo et al., 2008; Stokes et al., 2013; Rose et al., 2016).

Together with the earlier results showing that stronger alpha/beta amplitudes promote perceptual stability (i.e., longer-lasting percepts) during continuous bistable perception (Figure 4A), these results show that the neural mechanisms supporting perceptual memory localize to the same frequency bands, but have different circuit-level mechanisms. In addition, sensors supporting perceptual memory (when the stimulus is temporarily removed from view) reside in more anterior regions than those supporting perceptual stability (when the stimulus is in view) (compare topoplots between Figure 4A and 4B), suggesting that higher-order brain circuits are recruited to maintain a perceptual memory trace when sensory input is absent, consistent with previous fMRI findings (Wang et al., 2013).

DISCUSSION

In this study, we dissected the roles that different types of neural activity play in perception. We found evidence that perceptual content is predominantly encoded in the SCP (< 5Hz) range, and no evidence of perceptual content encoding in the amplitude of alpha and beta oscillations. This was the case regardless of whether the sensory input is ambiguous or unambiguous. We additionally found that SCP activity along with the amplitude of alpha and beta oscillations encoded aspects of perceptual switching, including the distance to a switch and whether the current percept is stabilizing or destabilizing. However, information about how long the current percept would last and whether a perceptual memory trace would occur if the stimulus is temporally removed from view was primarily encoded in alpha and beta amplitudes. Together, these results show a frequency-band separation of information related to perceptual content and perceptual stability, with the former encoded in raw fluctuations of low-frequency SCP activity, and the latter primarily influenced by the amplitude fluctuations of alpha and beta oscillations.

Previous studies on bistable perception have typically focused on one aspect of perceptual behavior at a time, such as perceptual content or perceptual switching. By using a novel neural state-space analysis approach, we were able to simultaneously extract components of neural activity relevant to different aspects of perceptual behavior that all vary across time/trials and are mutually independent. Additionally, this approach can uncover important relationships between neural activity underlying different aspects of behavior. For example, for alpha and beta amplitude, the

state space extracted for 'Blank' and 'Memory' axes in the *Discontinuous* condition are strongly correlated, suggesting a strong timing mechanism to how perceptual memory is encoded during the blank period (i.e., the neural activity pattern associated with the presence of a perceptual memory trace is similar to the activity pattern that increases over time during the blank period). Compared to other multivariate analysis methods, the neural state-space method has specific advantages and is well-suited to addressing the questions investigated herein. First, compared to multivariate decoding, the state-space method extracts multivariate neural activity patterns relevant to multiple behavioral metrics simultaneously, as opposed to investigating neural correlate of one behavioral metric at a time. Second, compared to automatic dimensionality reduction, such as PCA and similar techniques (Churchland et al., 2012; Cunningham and Yu, 2014; Baria et al., 2017), the state-space approach directly identifies the neural activity pattern (i.e. neural sub-space) relevant to a particular behavioral metric, as opposed to being behavior-agnostic.

Our finding of perceptual content-encoding in the SCP band provides further evidence of the role of SCP in conscious perception, consistent with earlier studies (Li et al., 2014; Baria et al., 2017; Flounders et al., 2019). A general role of SCP in supporting conscious awareness (He and Raichle, 2009) is also corroborated by recent findings comparing different states of consciousness (Bourdillon et al., 2020; Toker et al., 2022). In the domain of bistable perception, most studies probing neural correlates of perceptual content have employed fMRI [e.g., (Tong et al., 1998; Haynes and Rees, 2005; Wang et al., 2013)], and most electrophysiological studies have focused on changes in ERPs [e.g., (Britz et al., 2009; Pitts et al., 2009)], oscillatory power [e.g., (de Jong et al., 2016)] or neuronal firing rates (Gelbard-Sagiv et al., 2018) around perceptual switches. Previous electrophysiological studies probing neural correlates of perceptual content have typically used specialized stimulus design, such as frequency tagging (Tononi et al., 1998; Srinivasan et al., 1999), binocular rivalry involving face and oriented grating (where face-elicited ERFs, the M170, correlates with perceiving faces) (Sandberg et al., 2013; Sandberg et al., 2014), or auditory bistable stimuli where neural information integration correlates with perceiving an integrated auditory stream (Canales-Johnson et al., 2020). Here, by using classic ambiguous figures where the two percepts are symmetrical in salience and level of cortical processing, and showing results consistent across different images, our findings provide a more generalizable electrophysiological correlate of perceptual content. Our results also complement a recent intracranial electrophysiology study using the same ambiguous figures which revealed changes in corticocortical information flow depending on the specific perceptual content experienced (Hardstone et al., 2021). Finally, the potential role of gamma frequency band in encoding perceptual content should be further investigated in future studies using intracranial recordings which are more sensitive to gamma-band activity than MEG [e.g., (Panagiotaropoulos et al., 2012)].

A relationship between alpha and beta amplitudes and the stability of percepts has been reported in several previous studies of bistable perception (Kloosterman et al., 2015; Piantoni et al., 2017; Zhu et al., 2022). Although the detailed mechanisms involved remain unclear, two non-mutually-exclusive mechanisms have been proposed: lateral inhibition and the resulting dynamical attractor at a local scale (Piantoni et al., 2017) and top-down feedback from higher-order regions (Kloosterman et al., 2015; Zhu et al., 2022). While both local inhibition and top-down processing roles have been ascribed to alpha and beta oscillations (Jensen and Mazaheri, 2010; Michalareas et al., 2016; Spitzer and Haegens, 2017), we believe that our finding of higher alpha/beta amplitude being associated with stronger perceptual stability (Figure 4A) is more compatible with a top-down interpretation. While lateral inhibition between competing neuronal groups is a key ingredient of biophysical models of bistable perception [e.g., (Shpiro et al., 2009)], and enhancing cortical inhibition by administering lorazepam, a $GABA_A$ receptor agonist, enhances perceptual stability (van Loon et al., 2013), lorazepam also has the effect of reducing alpha power (Lozano-Soldevilla, 2018)—opposite to the present finding of a positive correlation between perceptual stability and alpha

power. By contrast, recent intracranial electrophysiological evidence suggests that top-down feedback can carry perceptual templates congruent with long-term priors that act to stabilize a particular percept (Hardstone et al., 2021). Given the well-documented role of alpha and beta oscillations in carrying top-down feedback (van Kerkoerle et al., 2014; Bastos et al., 2015; Michalareas et al., 2016), a plausible mechanism for the present finding of higher alpha/beta amplitudes being associated with longer percept durations is then a top-down modulatory influence carried in the alpha and beta bands.

Similarly, we interpret our finding of alpha and beta amplitudes being associated with perceptual memory as reflecting a top-down modulatory influence. Consistent with this interpretation, a previous fMRI study showed that the content of perception and perceptual memory during intermittent presentation of ambiguous images is especially decodable in higher-order frontoparietal regions, and that intermittent presentation elicits strong top-down influences as compared to continuous presentation (Wang et al., 2013). The locations of sensors involved in perceptual memory (Figure 4B) are more anterior than those involved in perceptual stability (Figure 4A), which may reflect the source and target of top-down modulation, respectively.

Our finding of alpha and beta amplitudes being related to perceptual memory is concordant with a recent EEG study (Zhu et al., 2022), but, superficially, the two studies appear to report opposite directions of this relationship: a negative correlation (manifested as negative β weights) in the present study vs. a positive correlation in the earlier EEG study. However, a closer inspection suggests that the two studies are in fact consistent: Zhu et al. used short blank durations (~0.5 – 1.5 sec), and alpha/beta amplitudes are higher in stable-blank trials than unstable-blank trials early (within 500-ms of blank-onset) during the blank period, but lower in stable-blank trials (after 800 ms) late in the blank periods (Fig. 4B therein). The present study used long blank durations (6 sec), and the lower alpha/beta amplitude in stable-blank trials is mostly evident at 500-ms following blank onset or later (Figure 4B, right, note 'projected average' is amplitude multiplied by β weights, which are negative). The exact neurophysiological mechanisms contributing to these time courses remain to be investigated, but both studies converge to suggest that alpha and beta amplitudes influence not only perceptual stability when sensory input is in view but also perceptual memory when sensory input is temporarily removed from view. Importantly, the presents results differ from previous studies showing beta power increases during working memory maintenance (Spitzer and Haegens, 2017), reinforcing the notion that perceptual memory differs from working memory: the former is unconscious and automatic (Pearson and Brascamp, 2008), while the latter is largely conscious and deliberate (Trubutschek et al., 2019). Furthermore, we found that neural activity (in the alpha and beta band) underlying perceptual memory has significant overlap with neural activity encoding elapsed time (as evidenced by a significant positive correlation of β weight vectors for the 'Blank' and 'Memory' axes), which also fits better with an automatic process as opposed to an working memory account (Souza and Oberauer, 2015; Fulvio and Postle, 2020).

In sum, across multiple perceptual conditions (unambiguous vs. ambiguous sensory input; continuous vs. intermittent presentation), we found that distinct components of dynamical neural activity contribute to the content vs. stability of perception. While perceptual content is encoded in the activity pattern of low-frequency neural activity in the SCP band, perceptual stability and perceptual memory are influenced by the fluctuations of alpha and beta oscillation amplitudes. These results provide clues to the neural mechanisms underlying stable visual experiences in the natural environment, wherein the ever-present noise and instability in the retinal images must be overcome to reconstruct the cause of sensory input in order to guide adaptive behavior. Finally, these results also inform future computational models of bistable visual perception and efforts to understand pathological processes underlying perceptual disorders in mental illnesses, including

abnormal bistable perceptual dynamics in autism and schizophrenia (Robertson et al., 2013; Kornmeier et al., 2017; Weilnhammer et al., 2020).

MATERIALS AND METHODS

Subjects

The experiment was approved by the Institutional Review Board of the National Institute of Neurological Disorders and Stroke (under protocol #14 N-0002). All subjects were right-handed and neurologically healthy with normal or corrected-to-normal vision. Nineteen subjects between 19 and 33 years of age (mean age 24.5; nine females) participated in the MEG experiment. We excluded one subject from analysis due to repeatedly falling asleep during the task. All subjects provided written informed consent.

Task design and behavioral analysis

The task was adapted from a previously run fMRI experiment (Wang et al., 2013). In the study, two well-known ambiguous images (Necker cube and Rubin face-vase) were used to study bistable perception under continuous (*Ambiguous* condition) and intermittent presentation (*Discontinuous* condition) (Figure 1). As a control, we also included a condition where we manipulated the content, outlines, and shading of the ambiguous images to accentuate one of the two percepts (*Unambiguous* condition), with the intention that the subject would perceive that percept.

Stimuli were presented using E-Prime Software (Psychology Software Tools, Sharpsburg, PA) via a Panasonic PT-D3500U projector with an ET-DLE400 lens, with the screen 55cm from the subject's eyes. All face-vase images subtended 16.9 × 17.6 (height x width) degrees of visual angle, and all cube images subtended 14.3 x 14.5 degree.

Each subject completed twelve runs, consisting of four sets of three runs in the following order: Unambiguous, Ambiguous, and Discontinuous conditions.

Each Ambiguous run contained six trials, with each trial consisting of 2 s of written instruction, 2 s of fixation (while fixating on a crosshair in the center of the screen), 60 s of image presentation, and 3-7 s of inter-trial interval (Figure 1A). Each ambiguous image was presented three times in a pseudorandom order. Subjects reported every spontaneous perceptual switch using their right hand via one of three buttons throughout the course of image presentation: one button for each of the possible percepts, and one for 'Unsure' which they were instructed to press if they experience neither or both of the possible percepts. In order to investigate spontaneous perceptual switches, subjects were instructed to passively view the images and not to try to switch or hold onto a percept.

Each Unambiguous run contained 32 trials, with each block consisting of 2 s of written instruction, 2 s of fixation, 5 s of image presentation, and 3-7 s of inter-trial interval (Figure 1C). The four unambiguous images were presented eight times each in a pseudorandom order. Subjects were asked to indicate their percept via one of three buttons (one button for each possible percept, and one for unsure) at each image presentation. Valid trials consisted of subjects pressing the button for the intended percept once, and no other button presses (Figure 1D).

Each Discontinuous run contained six trials, with each trial consisting of 2 s of written instruction, 2 s of fixation, nine repetitions of 2-s image presentation followed by a 6-s blank period (of which the last second contained the crosshair in the center of the screen) (Figure 1E). Subjects were asked to indicate their percept during each image presentation via a button press, and not to press buttons

during the blank period. Perceptual switching during the 2-s image presentation was very rare and was excluded from analyses. The two ambiguous images were presented in alternating trials.

For all conditions, subjects were instructed to fixate upon a crosshair at the center of the screen at all times to avoid the potential influence of gaze on perception. Response mapping was altered between runs, by switching the buttons for the two percepts. For the first 9 subjects the response mapping for the two percepts was switched after every run. For the final 10 subjects, we instead switched the response mapping after every set of 3 runs. Before entering the MEG, subjects performed practice runs until they were comfortable with the task and the buttons corresponding to each percept.

MEG Recordings

While performing the task, we recorded neural activity from each subject using a 275-channel whole-head MEG system (CTF). Three dysfunctional sensors were removed from all analyses. We also recorded gaze position and pupil size using a SR Research Eyelink 1000+ system. Eye-tracking was used for online monitoring of fixation and wakefulness during the experiment. MEG data were recorded at a sampling rate of 600 Hz, with a low-pass anti-aliasing filter of 150 Hz and no high-pass filter (i.e. DC recording). Before and after each run, the head position of a subject was measured using fiducial coils, in order to detect excessive movement. During each task subjects responded using a fibreoptic response button box. All MEG data samples were realigned with respect to the presentation delay of the projector (measured with a photodiode).

MEG data pre-processing and feature extraction

All pre-processing and analysis of data was performed in MATLAB (Mathworks, Natick, MA) using custom-written code and the FieldTrip toolbox (Oostenveld et al., 2011). MEG data were first demeaned and detrended. Data were then filtered at 0.05–150 Hz using a 3rd-order Butterworth filter, and line noise as well as harmonics were removed using 4th-order Butterworth band-stop filters (58–62, 118–122, 178–182 Hz). Independent component analysis (ICA, Fieldtrip *runica* method) was then applied, and components were manually inspected to remove those related to eye blinks, eye movements or heart-beat-related artifacts.

Three different features of neural activity were then extracted. Slow-cortical potential (SCP) activity was obtained using a 3rd-order low-pass Butterworth filter at 5 Hz. Alpha-band amplitude was extracted by taking the absolute of the Hilbert transform (Matlab, *abs(hilbert(data))*) of the pre-processed MEG data that had been filtered at 8–13 Hz using a 3rd-order Butterworth filter. Beta-band amplitude was extracted in the same way, but using data filtered in the 13–30 Hz range.

Decoding perceptual content

We attempted to decode perceptual content during the Ambiguous and Unambiguous conditions using the three extracted neural features (SCP, alpha amplitude, beta amplitude). For the *Ambiguous* condition, we first extracted periods between button presses where each button press was for a different percept (excluding 'Unsure' button presses), and the period was labelled according to the first button press (i.e. Face, Vase, Green or Blue). As these periods were all of different durations, we then rescaled them to be the same length by selecting 100 equally spaced time points, giving us percentiles of the percept's duration. For the *Unambiguous* condition we selected valid trials for analysis, wherein the subject only pressed a button once for the intended percept. The time period used for decoding was the 5 seconds that the image was on the screen, and MEG data were down-sampled to 10 Hz before applying the decoding pipeline. The label of the trial was the image that was presented (i.e. Face, Vase, Green or Blue). For both task conditions, the classification was done separately for the Necker Cube (Green vs. Blue) and Rubin Face-Vase (Face vs. vase). All trials were normalized (z-scored) across sensors at each time point. Trials were then split into 4 folds with an

equal number of trials of each label in each fold. Trials for a fold were selected by taking every 4th trial of that trial type (ordered by when the trial occurred during the recording).

The decoding pipeline consisted of taking one fold as the testing set, and training a linear support vector machine (SVM) classifier (cost = 1) using the LIBSVM packages (Chang and Lin, 2011) at each timepoint to the trials from the other three folds, which constituted the training set. Decoding accuracy of the classifier was then calculated on the testing set. The temporal cross-generalization of the classifier was also tested by assessing its classification accuracy at every other time point. This was done using each fold as the testing set, and the decoding accuracy (and temporal generalization) was averaged across the 4 folds.

Cluster-based permutation tests for multivariate pattern decoding

The group-level statistical significance of classifier accuracy at each time point was assessed by a one-tailed, one-sample Wilcoxon signed-rank test against chance level (50%). To correct for multiple comparisons, we used cluster-based permutation tests (Maris and Oostenveld, 2007). Temporal clusters were defined as contiguous time points with above-threshold classification accuracy (cluster-defining threshold: $p<0.1$). The test statistic W of the Wilcoxon signed-rank test was summed across time points in a cluster to yield a cluster's summary statistic. Cluster summary statistics were compared to a null distribution, constructed by shuffling class labels 100 times, and extracting the largest cluster summary statistic for each permutation. Clusters in original data with summary statistics exceeding the 95th percentile of null distribution were considered significant (corresponding to $p<0.05$, cluster-corrected, one-tailed test). For classifier temporal generalization, the permutation-based approach for cluster-level statistical inference used the same procedure as above, where clusters were defined as contiguous time points in training and/or generalization dimensions with above threshold ($p<0.1$) classification accuracy.

Neural state-space analysis

To work out the relative contributions of different behaviors to neural activity patterns, we developed a novel multivariate analysis method to extract the neural sub-space relevant to each behavior, following the approach used in (Mante et al., 2013). While perceptual content is clearly an important aspect of behavior, there are other aspects of behavior which account for the perceptual switching dynamics (*Ambiguous* condition) and perceptual memory (*Discontinuous* condition). For the *Ambiguous* condition, we first selected 100 equally spaced time-points from each period that occurred between button presses for the two percepts (i.e. not for time points preceded or followed by an unsure button press). We then defined 4 behavioral metrics for each time point:

- *Type*, a binary variable indicating the current percept.
- *Duration*, a continuous variable which takes the same value throughout a percept and is normalized within subject (i.e., 0 for the shortest percept reported, and 1 for the longest percept).
- *Switch*, a continuous variable that was 0 at the time of a button press and 1 at the midway point between button presses, indicating the relative temporal distance to perceptual switches.
- *Direction*, a binary variable indicating whether the current percept is stabilizing (i.e., timepoint is in the first half of its duration) or destabilizing (i.e., in the second half of its duration).

For the *Discontinuous* condition, only time points during the blank period (6 sec total, including the 1-sec fixation period) were used, where the blank period was preceded and followed by an image presentation during which the subject pressed for one of the two percepts. Four behavioral metrics were defined:

- *Pre*, a binary variable indicating the percept reported before the blank period
- *Post*, a binary variable indicating the percept reported after the blank period

- *Blank*, a continuous variable increasing from 0 at the beginning of the blank period to 1 at the end of the blank period, indicating time elapsed during the blank period
- *Memory*, a binary variable indicating whether the percept before the blank was the same as that after the blank, with 1 indicating the presence of a memory trace and 0 indicating the absence of a memory trace.

These time points were split into two data sets (1st and 2nd half of timepoints based on time through experiment), with the first half used as the training set, and the second half used as the test set. Using the training data set, the MEG data (applied separately for the three neural features: SCP, alpha amplitude and beta amplitude) for each sensor is first normalized over time using the mean and standard deviation from the training set. A multi-linear regression of the following form was solved to find the β weights in the equation (using MATLAB function *fitlm*, with *RobustOpts)*:

$$MEG_{sensor1} = \beta_{a1}Behavior_a + \beta_{b1}Behavior_b + \beta_{c1}Behavior_c + \beta_{d1}Behavior_d + \varepsilon$$

These β weights define the axes of the behavioral subspace for that neural feature. MEG data from the test set (which has been normalized at the individual sensor level using the mean and standard deviation from the training set, so that the projection method does not depend on any information from the test set) can then be projected onto the behavioral axes (using the MATLAB function *mldivide*). This gives a prediction of the value for each behavioral metric based on neural activity at each time point of the test set.

Statistics for neural state-space analysis

To assess the consistency across subjects of the β weights defining each behavioral axis, and whether each neural feature carried predictive information about the behavior, a cluster-based permutation method (Maris and Oostenveld, 2007) was applied separately for each axis. This involved shuffling the behavioral information across all of the trials only for that axis. For axes where behavior was defined in the same way for each trial (Ambiguous: Switch and Direction Axes. Discontinuous: Blank Axis), each trial was instead "flipped" with a 50% chance, where the flipped trial was equal to 1 – original behavior. Once the behavioral data was shuffled, the state-space analysis was re-applied, and this was done for 100 permutations of the data.

To assess consistency of the β weights defining each behavioral axis, a two-sided Wilcoxon sign-rank test against zero was applied separately to each electrode. To correct for multiple comparisons across sensors, we used cluster-based permutation tests (Maris and Oostenveld, 2007). Spatially contiguous electrodes with a significant bias (p<0.05) and the same sign of the test statistic W, formed a cluster (either positive or negative depending on the sign) where the cluster summary statistic was the sum of the electrodes' test statistic W. This cluster summary statistic was compared to a null distribution, formed from the largest (i.e., most positive or most negative) cluster summary statistic for each permutation. Clusters in original data with summary statistics exceeding the 95th percentile of null distribution were considered significant (corresponding to p<0.05, cluster-corrected, one-tailed test). Positive and negative clusters were assessed separately by comparison to the respective null distribution.

To assess consistency between two state-spaces (either between β weight maps for the two different images and the same axis, or between two different axes and the same image), cosine similarity was applied:

$$\cos\theta = \frac{\boldsymbol{\beta_A} \cdot \boldsymbol{\beta_B}}{\|\boldsymbol{\beta_A}\| \|\boldsymbol{\beta_B}\|}$$

where $\boldsymbol{\beta_A}$ and $\boldsymbol{\beta_B}$ correspond to the two β weight maps. Cosine similarity produces a value between -1 and 1, where 1 indicates that the projection of the MEG data into the two behavioral state-spaces

would produce perfectly correlated behavioral estimates, and -1 indicates that they would be entirely anti-correlated. To assess significance of the cosine similarity, a null distribution was created by calculating cosine similarity between the two β maps for each permutation, and the *p*-value was calculated as the fraction of this distribution with values larger than the cosine similarity of the original data.

To assess whether each neural feature carried predictive information about each behavioral axis, a different test was applied depending on the axis. In the following analyses, a one-sided statistical test is often used because if the neural subspace is successfully extracted, the predicted behavioral metric in the test dataset should follow specific relationships similar to the definition of these axes (Figure 3A).

First, data from the test data set were projected into the neural subspace defined for each axis using the training data. For those axes with binary behavior that had the same value across time for each trial (Ambiguous: Type; Discontinuous: Pre, Post), a paired t-test across subjects (one-sided) was applied at each time point between the trial-averaged predicted behavior for the two groups of trials (e.g. Green Cube and Blue Cube).

For the axis with continuous behavior that had the same value across time for each trial (Ambiguous: Duration), two analyses were carried out: 1) (Figure 4A) For each subject, predicted percept duration (using neural activity at each time point) was correlated with the actual percept duration across trials by a Spearman correlation. The rho-values were then subjected to a Wilcoxon sign-rank test across subjects (one-sided), and corrected for multiple comparisons using cluster-based permutation test.
a one-sided Wilcoxon sign-rank test was applied at each time point between the predicted and actual behavior. 2) (Figure 4—figure supplement 1B) A median split was performed on the test data set for each subject according to percept duration. The projected data (i.e., predicted percept duration based on neural data) were then compared between the two groups of trials by a paired t-test across subjects (one-sided), and corrected for multiple comparisons using cluster-based permutation test.

For those axes where the actual behavior changed across time within a trial in a continuous manner (Ambiguous: Switch; Discontinuous: Blank), the trial-averaged predicted behavior from each subject was compared to the actual behavior using a Spearman correlation. The Spearman rho values were then subjected to a group-level test using a Wilcoxon signed-rank test against zero (one-sided).

Lastly, for the axis where actual behavior changed across a trial in a binary manner (Ambiguous: Direction), the trial-averaged predicted behavior for each subject was compared between the first half of the trial and the second half of the trial using a two-sample t-test. The resulting t-values were then subjected to a Wilcoxon signed-rank test against zero (one-sided) at the group level.

To correct for multiple comparisons, we used cluster-based permutation tests (Maris and Oostenveld, 2007). Temporal clusters were defined as contiguous time points with above-threshold test statistic (cluster-defining threshold: $p<0.05$). The test statistic (Wilcoxon signed rank (W) or t-test (t)) was summed across time points in a cluster to yield a cluster's summary statistic. Cluster summary statistics were compared to a null distribution, formed by extracting the largest cluster summary statistic for each permutation. Clusters in original data with summary statistics exceeding the 95th percentile of null distribution were considered significant (corresponding to $p<0.05$, cluster-corrected, one-tailed test).

ACKNOWLEDGMENTS

This work was supported by a National Science Foundation CAREER Award (BCS-1753218), an Irma T. Hirschl Career Scientist Award, and a National Institutes of Health grant (R01EY032085) to B.J.H.. M.Z. was supported by NIH Training Grant R90DA043849.

CONFLICTS OF INTEREST

No Conflicts of Interest declared.

DATA AVAILABILITY

Data and code to reproduce the figures are available at figshare repository:
https://figshare.com/s/c328299bea96686c2eec

FIGURES

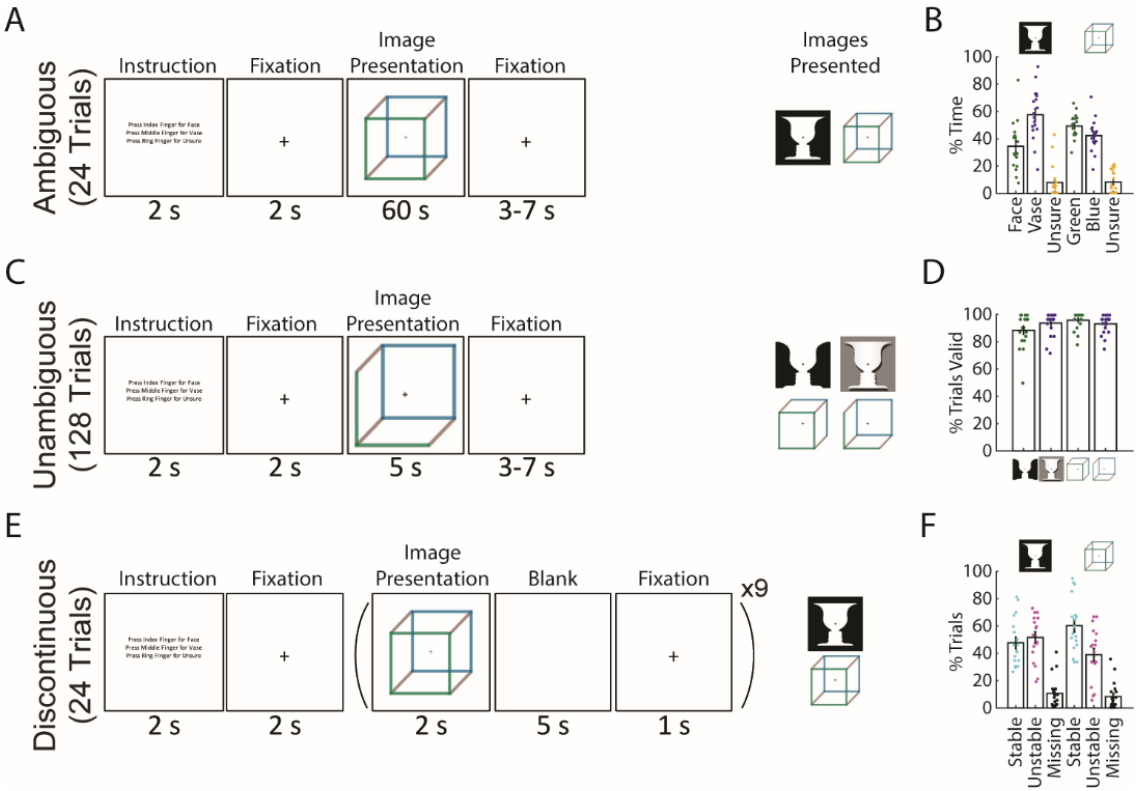

Figure 1. Paradigm and behavioral results. (A) In the *Ambiguous* condition, bistable images were presented for 60 seconds each, and subjects pressed buttons to indicate their current percept. **(B)** Percentage of time spent in each perceptual state during the *Ambiguous* condition. **(C)** In the *Unambiguous* condition, bistable images which were modified to reduce their ambiguity were presented. **(D)** Percentage of valid trials for each image type during the Unambiguous condition. Valid trials consisted of the subject pressing the button only once for the intended percept. **(E)** In the *Discontinuous* condition, ambiguous images were shown 9 times with interleaving blank periods. **(F)** Percentage of Blank periods that were classified as Stable, Unstable or Missing. 'Stable' indicates that perception was the same before and after the blank period, 'Unstable' that it was different, and 'missing' indicates that no button press was recorded during the pre or post image-presentation period. (**B,D,F**) Dots indicate individual subjects; bars and error bars indicate group mean and s.e.m.

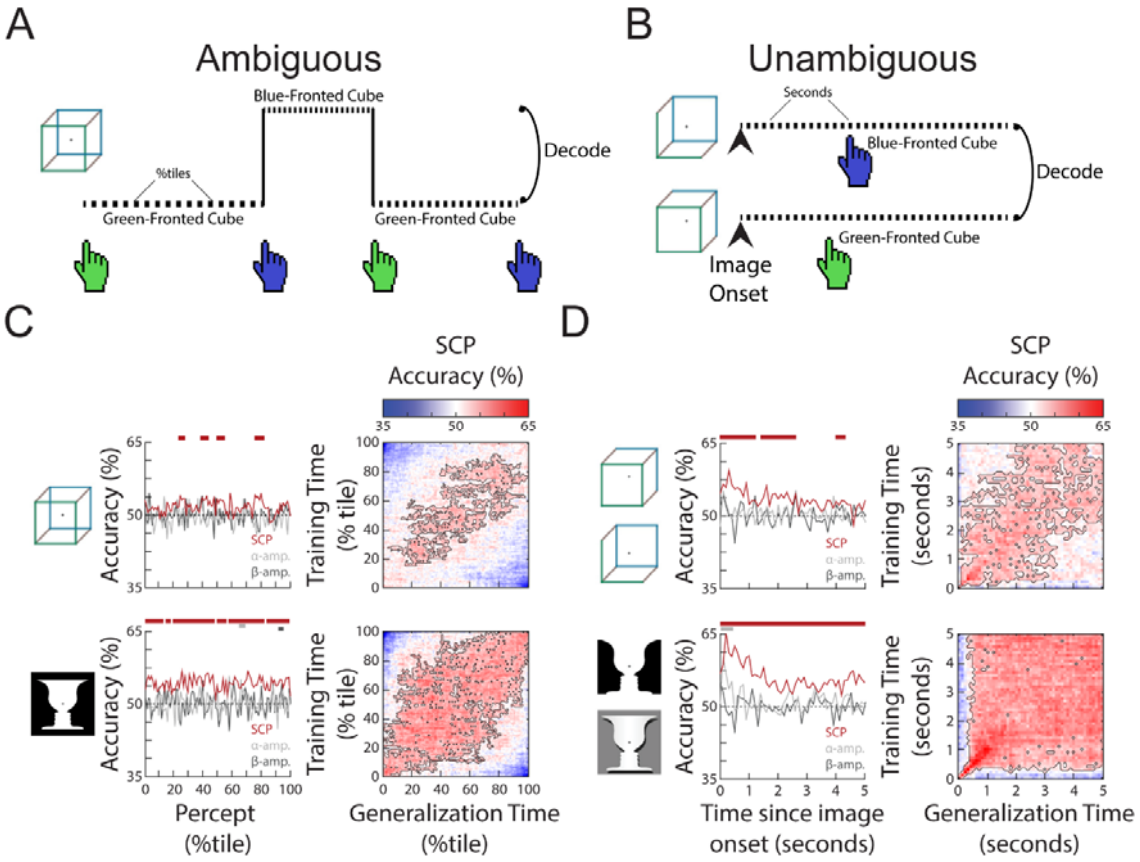

765
766
767 **Figure 2. The content of subjective perception is encoded in SCP activity. (A)** In the *Ambiguous*
768 condition, subjects continuously reported their current perception using button presses. Neural
769 activity during each percept was split into 100 percentiles according to time elapsed, and percept
770 was then decoded at each temporal percentile. **(B)** In the *Unambiguous* condition, different
771 disambiguated images were shown that emphasized one of the two percepts. For valid trials in
772 which subjects' reported percept matched the intended percept (see Fig. 1D), image content was
773 decoded separately at each timepoint during image presentation. **(C)** (*Left*) Decoding accuracy for
774 perceptual content during the time course of a percept. Significant temporal clusters of percept
775 decoding exist for both images using SCP as the decoder input, but not when alpha or beta
776 amplitude was used as decoder input. (*Right*) Temporal generalization matrices. Significant clusters
777 are outlined, showing generalization across a large proportion of the percept duration. **(D)** (*Left*)
778 Decoding accuracy for unambiguous images during their presentation. Significant temporal clusters
779 of image/percept decoding exist in the SCP range throughout image presentation, but not for
780 alpha/beta amplitude. (*Right*) Temporal generalization matrices showing significant generalization
781 across a large proportion of the image presentation duration.
782

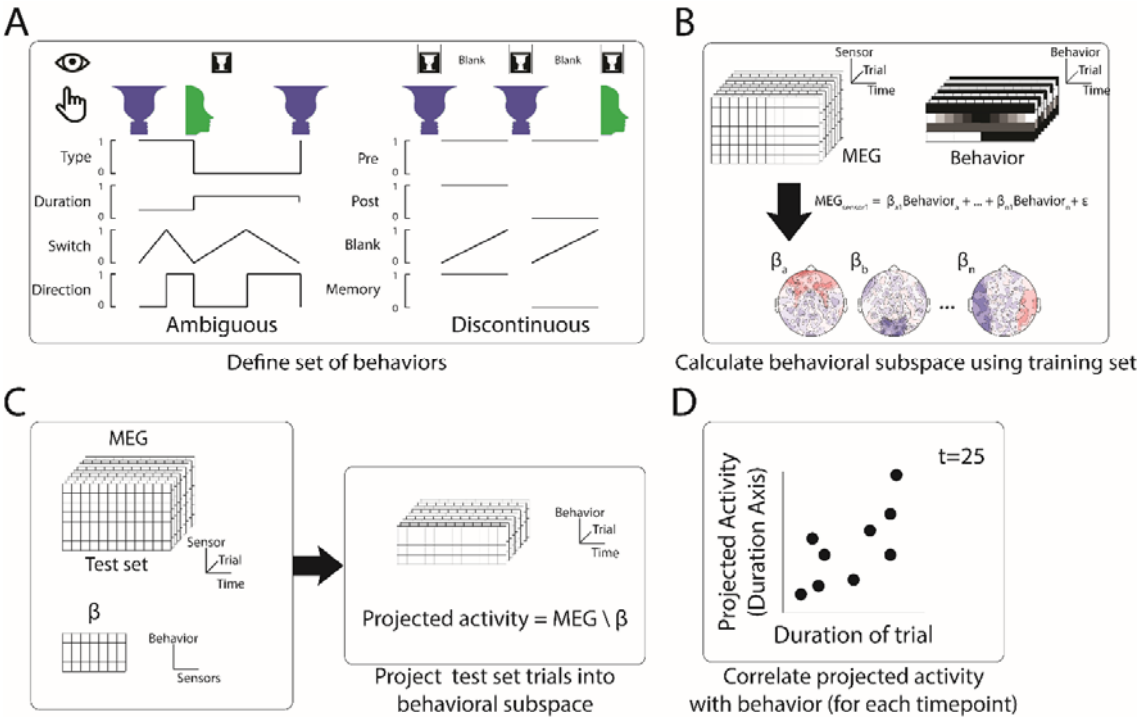

Figure 3. Method to define behaviorally relevant neural subspace. (A) For the *Ambiguous* and *Discontinuous* conditions a set of behavioral metrics was defined, which incorporated information about both the perceptual content and the perceptual switching dynamics. **(B)** Using a training set of MEG data, neural subspaces were defined by apply multi-linear regression to activity from each sensor using the four behavioral metrics as predictors. The weights across sensors for each behavioral metric define the neural subspace relevant to that metric. **(C)** The test MEG dataset can then be projected into the subspace corresponding to a particular behavioral metric to provide a prediction of the metric value at each timepoint. **(D)** Accuracy of the prediction can then be tested by comparison to the actual behavioral data.

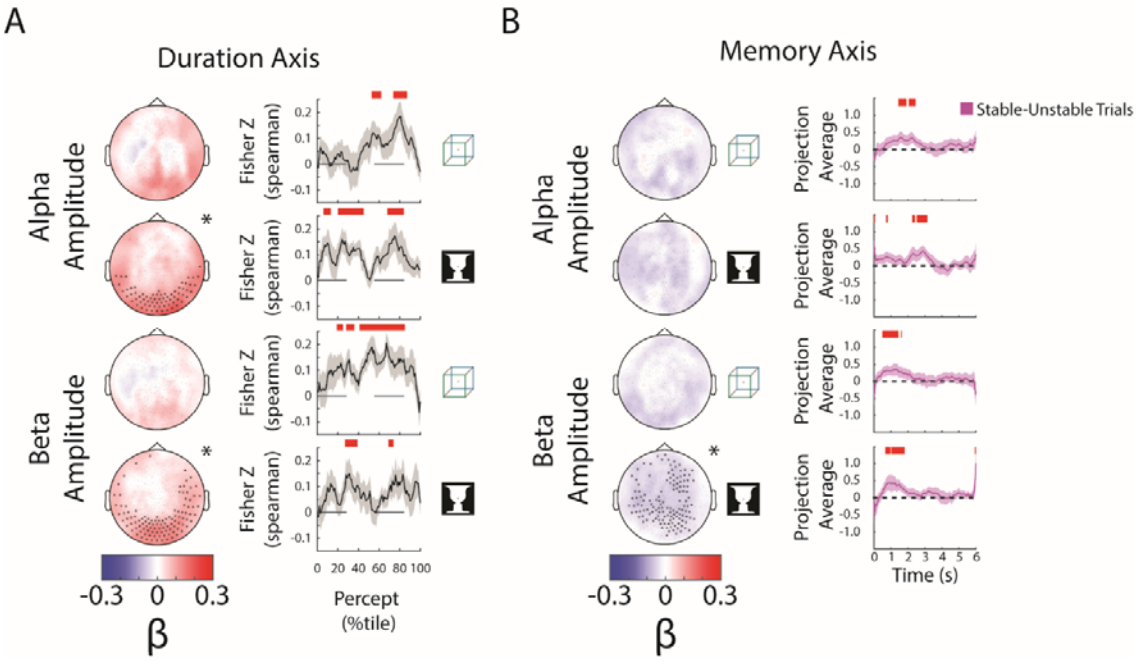

Figure 4. Alpha and beta amplitudes are involved in the switching process and perceptual memory trace. (A) (*Left*) Group-average β weights for Duration axis in the ambiguous condition. Sensors whose β weights are significantly different from zero (Wilcoxon signed-rank test, cluster-corrected, $p<0.05$) are marked with x. (*Right*) Mean Fisher z-transformed Spearman rho values, obtained by correlating predicted and actual behavioral values across trials for each subject. Shaded areas show group-level s.e.m. Significant time points ($p<0.05$, cluster-based permutation test) are indicated by the horizontal red bars. (**B)** (*Left*) Group-average β weights for Memory axis in the discontinuous condition. Sensors whose group-level β weights are significantly different from zero (Wilcoxon signed-rank test, cluster-corrected, $p<0.05$) are marked with x. (*Right*) Difference in neural activity projected onto the Memory axis between the Stable and Unstable trials (i.e., blank periods sandwiched by the same percept or different percepts). Significant differences ($p<0.05$, cluster-based permutation test) between them are indicated by red horizontal bars.

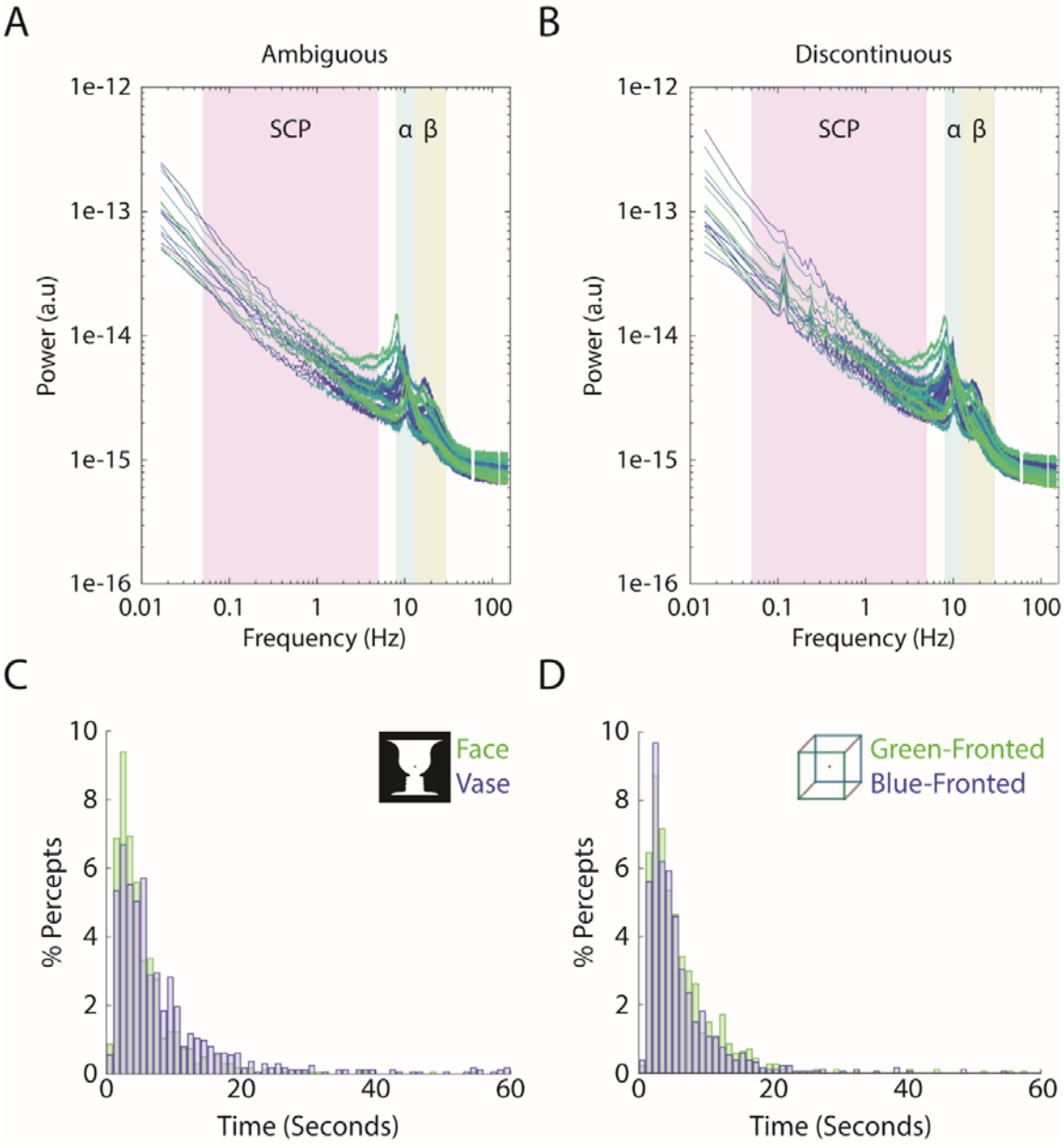

811

812 **Figure 1—figure supplement 1. Individual-level power spectra, and group level duration**
813 **histograms. (A,B)** Each line corresponds to a subject's power spectrum averaged over all 272 MEG
814 sensors. Shaded boxes correspond to the three frequency bands analyzed, SCP (0.05-5Hz), alpha (8-
815 13 Hz) amplitude, and beta (13-30 Hz) amplitude. For the discontinuous condition, peaks can be seen
816 in low frequencies corresponding to the task structure (8 seconds between consecutive image
817 onsets gives rise to 0.125 Hz and its harmonics). Frequencies at line noise (60 Hz) and its harmonics
818 are not plotted. **(C,D)** Histograms showing the distribution of percept durations, including data
819 pooled across 19 subjects.
820

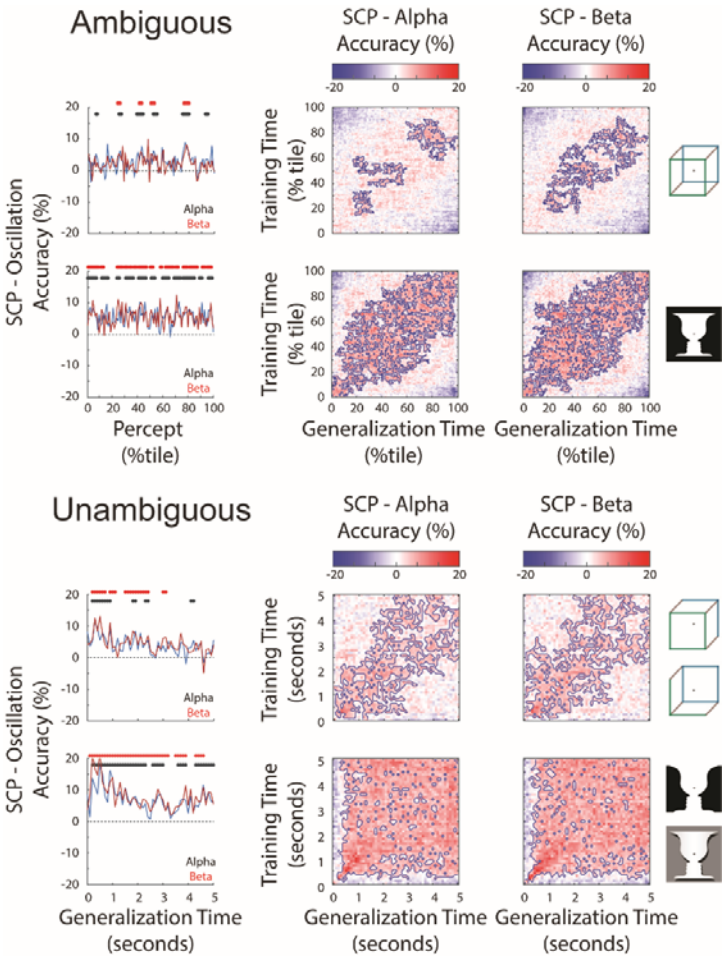

Figure 2—figure supplement 1. SCP has significantly higher decoding than alpha or beta oscillations in both the ambiguous (top) and unambiguous (bottom) conditions. (*Left*) Difference in decoding accuracy between SCP and alpha/beta amplitude for perceptual content across the time course of a percept. Significant temporal clusters of percept decoding exist for both images. (*Right*) Difference in temporal generalization matrices (SCP – alpha or beta amplitude). Significant clusters are outlined, showing the temporal-generalization locations where SCP has significantly greater decoding accuracy. Significance for all plots is established by cluster-based permutation test and presented at a $p < 0.05$, corrected level.

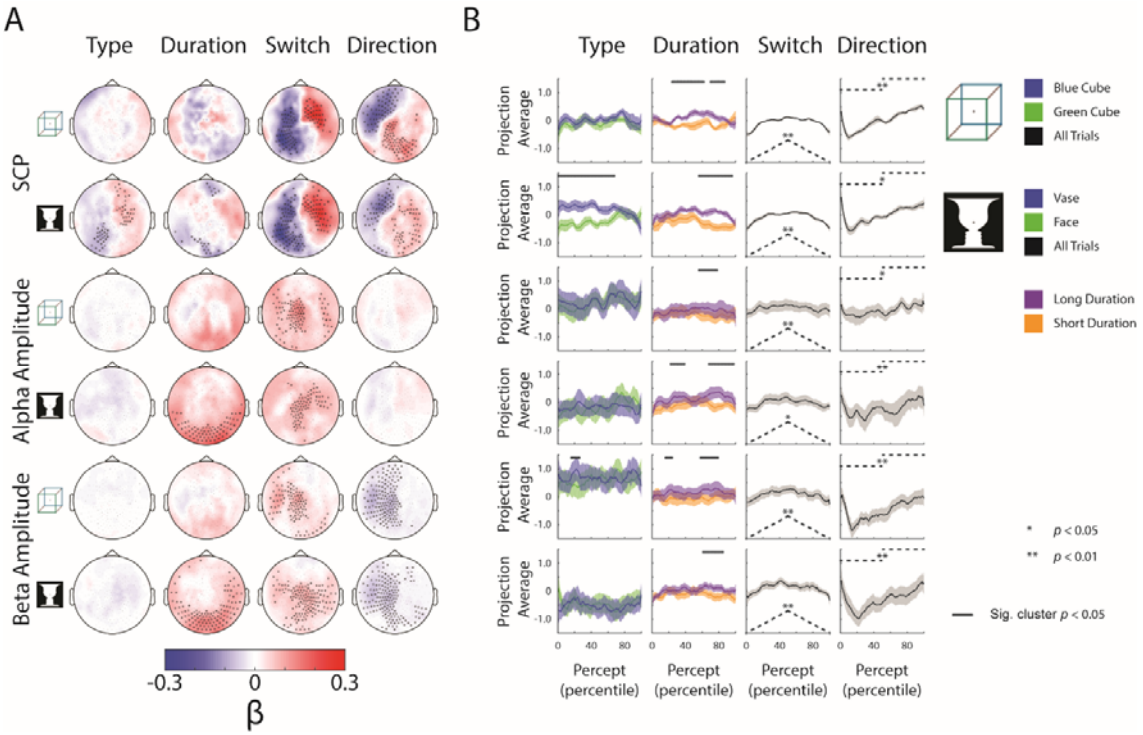

Figure 4—figure supplement 1. Complete neural subspace results for the *Ambiguous* condition. (A) Group-average β weights. Sensors whose β weights are significantly different from zero (Wilcoxon signed-rank test, cluster-corrected, p<0.05) are marked with x. **(B)** Test data set projected onto each behavioral axis; shaded areas indicate s.e.m. across subjects. For the. Type axis, trials for the different percepts are projected and averaged separately, and difference between the trial-averaged projections are tested by a paired t-test across subjects (one-sided). For the Duration axis, the longest and shortest 50% of trials are averaged and compared by a paired t-test across subjects (one-sided). Significant temporal clusters (p<0.05, cluster-based permutation test) are indicated by black horizontal bars at the top. For the Switch and Direction axes, all trials are projected and averaged, and compared to the actual behavioral metric (shown as dashed black lines here, also see Fig. 3A) using a Spearman correlation for the Switch axis and a two-sample t-test (between the 1st and 2nd half of the trial) for the Direction axis. Subsequently, the rho and t-stats are tested at the group level by a Wilcoxon sign-rank test against zero (one-sided).

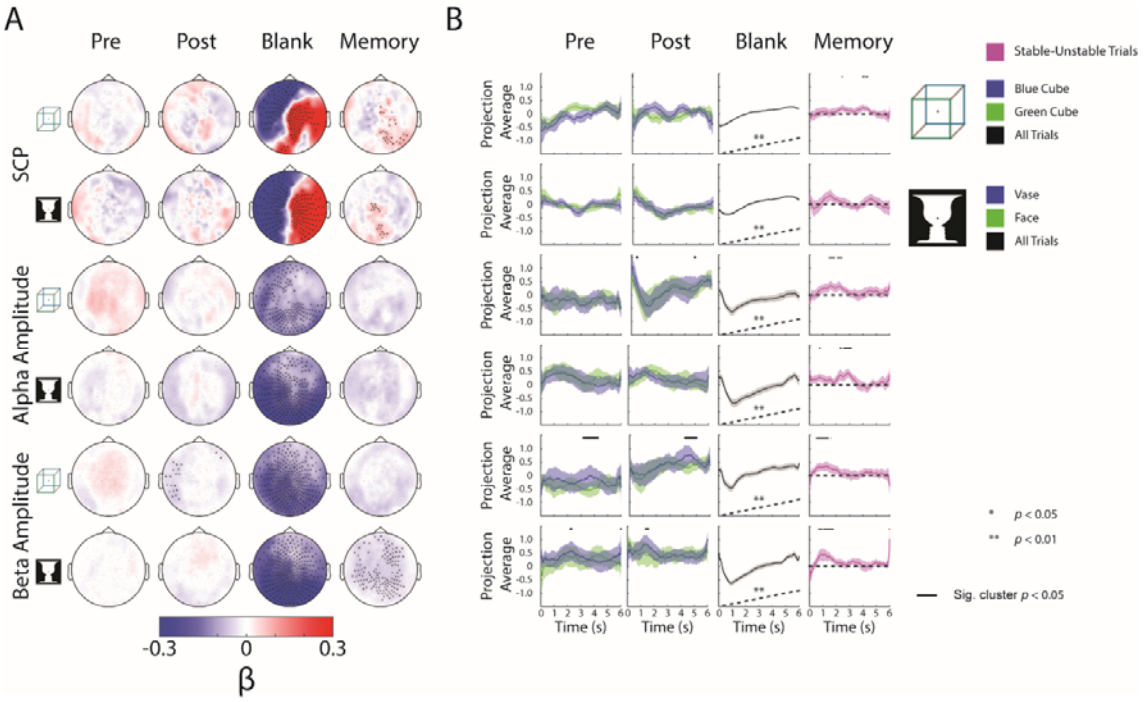

Figure 4—figure supplement 2. Complete neural subspace results for the *Discontinuous* condition. **(A)** Group-average β weights. Sensors whose β weights are significantly different from zero (Wilcoxon signed-rank test, cluster-corrected, p<0.05) are marked with x. (**B)** Test data set, including data from the blank periods only, projected onto each behavioral axis; shaded areas indicate s.e.m. across subjects. For Pre and Post axes, trials for the different percepts are projected separately, and difference between them tested by a paired t-test (one-sided) across subjects. For the Blank axis, all trials are projected and averaged and compared to the actual behavior (shown as black dashed line here; also see Fig. 3A) using a Spearman correlation; subsequently, the *rho* values were tested at the group level by a Wilcoxon sign-rank test against zero (one-sided). For the Memory axis, stable and unstable trials are projected separately, and the difference between them is plotted and tested by a one-sample t-test across subjects (one-sided).

REFERENCES

Baria AT, Maniscalco B, He BJ (2017) Initial-state-dependent, robust, transient neural dynamics encode conscious visual perception. PLoS Comput Biol 13:e1005806.

Bastos AM, Vezoli J, Bosman CA, Schoffelen JM, Oostenveld R, Dowdall JR, De Weerd P, Kennedy H, Fries P (2015) Visual Areas Exert Feedforward and Feedback Influences through Distinct Frequency Channels. Neuron 85:390-401.

Bourdillon P, Hermann B, Guenot M, Bastuji H, Isnard J, King JR, Sitt J, Naccache L (2020) Brain-scale cortico-cortical functional connectivity in the delta-theta band is a robust signature of conscious states: an intracranial and scalp EEG study. Sci Rep 10:14037.

Briggman KL, Abarbanel HD, Kristan WB, Jr. (2005) Optical imaging of neuronal populations during decision-making. Science 307:896-901.

Britz J, Landis T, Michel CM (2009) Right parietal brain activity precedes perceptual alternation of bistable stimuli. Cereb Cortex 19:55-65.

Canales-Johnson A, Billig AJ, Olivares F, Gonzalez A, Garcia MDC, Silva W, Vaucheret E, Ciraolo C, Mikulan E, Ibanez A, Huepe D, Noreika V, Chennu S, Bekinschtein TA (2020) Dissociable Neural Information Dynamics of Perceptual Integration and Differentiation during Bistable Perception. Cereb Cortex 30:4563-4580.

Carlson T, Tovar DA, Alink A, Kriegeskorte N (2013) Representational dynamics of object vision: the first 1000 ms. J Vis 13.

Cavanagh P (1991) What's up in top-down processing? In: Representation of Vision: Trends and Tacit Assumptions in Vision Research (A G, ed), pp 295-304.

Chang C-C, Lin C-J (2011) LIBSVM : a library for support vector machines. . ACM Transactions on Intelligent Systems and Technology, 2:1-27.

Churchland MM, Cunningham JP, Kaufman MT, Foster JD, Nuyujukian P, Ryu SI, Shenoy KV (2012) Neural population dynamics during reaching. Nature 487:51-56.

Cunningham JP, Yu BM (2014) Dimensionality reduction for large-scale neural recordings. Nat Neurosci 17:1500-1509.

de Jong MC, Hendriks RJ, Vansteensel MJ, Raemaekers M, Verstraten FA, Ramsey NF, Erkelens CJ, Leijten FS, van Ee R (2016) Intracranial Recordings of Occipital Cortex Responses to Illusory Visual Events. J Neurosci 36:6297-6311.

Donoghue T, Haller M, Peterson EJ, Varma P, Sebastian P, Gao R, Noto T, Lara AH, Wallis JD, Knight RT, Shestyuk A, Voytek B (2020) Parameterizing neural power spectra into periodic and aperiodic components. Nat Neurosci 23:1655-1665.

Flounders MW, Gonzalez-Garcia C, Hardstone R, He BJ (2019) Neural dynamics of visual ambiguity resolution by perceptual prior. eLife 8.

Fulvio JM, Postle BR (2020) Cognitive Control, Not Time, Determines the Status of Items in Working Memory. J Cogn 3:8.

Gelbard-Sagiv H, Mudrik L, Hill MR, Koch C, Fried I (2018) Human single neuron activity precedes emergence of conscious perception. Nature communications 9:2057.

Hardstone R, Zhu M, Flinker A, Melloni L, Devore S, Friedman D, Dugan P, Doyle WK, Devinsky O, He BJ (2021) Long-term priors influence visual perception through recruitment of long-range feedback. Nature communications 12:6288.

Haufe S, Meinecke F, Gorgen K, Dahne S, Haynes JD, Blankertz B, Biessmann F (2014) On the interpretation of weight vectors of linear models in multivariate neuroimaging. Neuroimage 87:96-110.

Haynes JD, Rees G (2005) Predicting the stream of consciousness from activity in human visual cortex. Curr Biol 15:1301-1307.

He BJ (2014) Scale-free brain activity: past, present, and future. Trends Cogn Sci 18:480-487.

He BJ, Raichle ME (2009) The fMRI signal, slow cortical potential and consciousness. Trends Cogn Sci 13:302-309.

912 He BJ, Zempel JM, Snyder AZ, Raichle ME (2010) The temporal structures and functional significance
913 of scale-free brain activity. Neuron 66:353-369.
914 Jensen O, Mazaheri A (2010) Shaping functional architecture by oscillatory alpha activity: gating by
915 inhibition. Front Hum Neurosci 4:186.
916 Kayser SJ, McNair SW, Kayser C (2016) Prestimulus influences on auditory perception from sensory
917 representations and decision processes. Proc Natl Acad Sci U S A 113:4842-4847.
918 King JR, Dehaene S (2014) Characterizing the dynamics of mental representations: the temporal
919 generalization method. Trends Cogn Sci 18:203-210.
920 King JR, Pescetelli N, Dehaene S (2016) Brain Mechanisms Underlying the Brief Maintenance of Seen
921 and Unseen Sensory Information. Neuron 92:1122-1134.
922 Kloosterman NA, Meindertsma T, Hillebrand A, van Dijk BW, Lamme VA, Donner TH (2015) Top-
923 down modulation in human visual cortex predicts the stability of a perceptual illusion. J
924 Neurophysiol 113:1063-1076.
925 Kornmeier J, Worner R, Riedel A, Tebartz van Elst L (2017) A different view on the Necker cube-
926 Differences in multistable perception dynamics between Asperger and non-Asperger
927 observers. PLoS One 12:e0189197.
928 Leopold DA, Wilke M, Maier A, Logothetis NK (2002) Stable perception of visually ambiguous
929 patterns. Nat Neurosci 5:605-609.
930 Li Q, Hill Z, He BJ (2014) Spatiotemporal dissociation of brain activity underlying subjective
931 awareness, objective performance and confidence. J Neurosci 34:4382-4395.
932 Lozano-Soldevilla D (2018) On the Physiological Modulation and Potential Mechanisms Underlying
933 Parieto-Occipital Alpha Oscillations. Frontiers in computational neuroscience 12:23.
934 Mante V, Sussillo D, Shenoy KV, Newsome WT (2013) Context-dependent computation by recurrent
935 dynamics in prefrontal cortex. Nature 503:78-84.
936 Maris E, Oostenveld R (2007) Nonparametric statistical testing of EEG- and MEG-data. J Neurosci
937 Methods 164:177-190.
938 Michalareas G, Vezoli J, van Pelt S, Schoffelen JM, Kennedy H, Fries P (2016) Alpha-Beta and Gamma
939 Rhythms Subserve Feedback and Feedforward Influences among Human Visual Cortical
940 Areas. Neuron 89:384-397.
941 Mongillo G, Barak O, Tsodyks M (2008) Synaptic theory of working memory. Science 319:1543-1546.
942 Nobre AC, van Ede F (2018) Anticipated moments: temporal structure in attention. Nat Rev Neurosci
943 19:34-48.
944 Oostenveld R, Fries P, Maris E, Schoffelen JM (2011) FieldTrip: Open source software for advanced
945 analysis of MEG, EEG, and invasive electrophysiological data. Computational intelligence and
946 neuroscience 2011:156869.
947 Orbach J, Zucker E, Olson R (1966) Reversibility of the necker cube: VII. Reversal rate as a function of
948 figure-on and figure-off durations. Percept Mot Skills 22:615-618.
949 Panagiotaropoulos TI, Deco G, Kapoor V, Logothetis NK (2012) Neuronal discharges and gamma
950 oscillations explicitly reflect visual consciousness in the lateral prefrontal cortex. Neuron
951 74:924-935.
952 Pearson J, Brascamp J (2008) Sensory memory for ambiguous vision. Trends Cogn Sci 12:334-341.
953 Piantoni G, Romeijn N, Gomez-Herrero G, Van Der Werf YD, Van Someren EJW (2017) Alpha Power
954 Predicts Persistence of Bistable Perception. Sci Rep 7:5208.
955 Pitts MA, Martinez A, Stalmaster C, Nerger JL, Hillyard SA (2009) Neural generators of ERPs linked
956 with Necker cube reversals. Psychophysiology 46:694-702.
957 Robertson CE, Kravitz DJ, Freyberg J, Baron-Cohen S, Baker CI (2013) Slower rate of binocular rivalry
958 in autism. J Neurosci 33:16983-16991.
959 Rose NS, LaRocque JJ, Riggall AC, Gosseries O, Starrett MJ, Meyering EE, Postle BR (2016)
960 Reactivation of latent working memories with transcranial magnetic stimulation. Science
961 354:1136-1139.

962 Salti M, Monto S, Charles L, King JR, Parkkonen L, Dehaene S (2015) Distinct cortical codes and
963 temporal dynamics for conscious and unconscious percepts. eLife 4.
964 Samaha J, Iemi L, Haegens S, Busch NA (2020) Spontaneous Brain Oscillations and Perceptual
965 Decision-Making. Trends Cogn Sci 24:639-653.
966 Sandberg K, Bahrami B, Kanai R, Barnes GR, Overgaard M, Rees G (2013) Early visual responses
967 predict conscious face perception within and between subjects during binocular rivalry. J
968 Cogn Neurosci 25:969-985.
969 Sandberg K, Barnes GR, Bahrami B, Kanai R, Overgaard M, Rees G (2014) Distinct MEG correlates of
970 conscious experience, perceptual reversals and stabilization during binocular rivalry.
971 Neuroimage 100:161-175.
972 Shpiro A, Moreno-Bote R, Rubin N, Rinzel J (2009) Balance between noise and adaptation in
973 competition models of perceptual bistability. J Comput Neurosci 27:37-54.
974 Souza AS, Oberauer K (2015) Time-based forgetting in visual working memory reflects temporal
975 distinctiveness, not decay. Psychon Bull Rev 22:156-162.
976 Spitzer B, Haegens S (2017) Beyond the Status Quo: A Role for Beta Oscillations in Endogenous
977 Content (Re)Activation. eNeuro 4.
978 Srinivasan R, Russell DP, Edelman GM, Tononi G (1999) Increased synchronization of neuromagnetic
979 responses during conscious perception. J Neurosci 19:5435-5448.
980 Stokes MG, Kusunoki M, Sigala N, Nili H, Gaffan D, Duncan J (2013) Dynamic coding for cognitive
981 control in prefrontal cortex. Neuron 78:364-375.
982 Sussillo D (2014) Neural circuits as computational dynamical systems. Curr Opin Neurobiol 25:156-
983 163.
984 Toker D, Pappas I, Lendner JD, Frohlich J, Mateos DM, Muthukumaraswamy S, Carhart-Harris R, Paff
985 M, Vespa PM, Monti MM, Sommer FT, Knight RT, D'Esposito M (2022) Consciousness is
986 supported by near-critical slow cortical electrodynamics. Proc Natl Acad Sci U S A 119.
987 Tong F, Nakayama K, Vaughan JT, Kanwisher N (1998) Binocular rivalry and visual awareness in
988 human extrastriate cortex. Neuron 21:753-759.
989 Tononi G, Srinivasan R, Russell DP, Edelman GM (1998) Investigating neural correlates of conscious
990 perception by frequency-tagged neuromagnetic responses. Proc Natl Acad Sci U S A
991 95:3198-3203.
992 Trubutschek D, Marti S, Ueberschar H, Dehaene S (2019) Probing the limits of activity-silent non-
993 conscious working memory. Proc Natl Acad Sci U S A 116:14358-14367.
994 van Kerkoerle T, Self MW, Dagnino B, Gariel-Mathis MA, Poort J, van der Togt C, Roelfsema PR
995 (2014) Alpha and gamma oscillations characterize feedback and feedforward processing in
996 monkey visual cortex. Proc Natl Acad Sci U S A 111:14332-14341.
997 van Loon AM, Knapen T, Scholte HS, St John-Saaltink E, Donner TH, Lamme VA (2013) GABA shapes
998 the dynamics of bistable perception. Curr Biol 23:823-827.
999 Wang M, Arteaga D, He BJ (2013) Brain mechanisms for simple perception and bistable perception.
1000 Proc Natl Acad Sci U S A 110:E3340-E3349.
1001 Weilnhammer V, Rod L, Eckert AL, Stuke H, Heinz A, Sterzer P (2020) Psychotic Experiences in
1002 Schizophrenia and Sensitivity to Sensory Evidence. Schizophr Bull 46:927-936.
1003 Yuille A, Kersten D (2006) Vision as Bayesian inference: analysis by synthesis? Trends Cogn Sci
1004 10:301-308.
1005 Zhu M, Hardstone R, He BJ (2022) Neural oscillations promoting perceptual stability and perceptual
1006 memory during bistable perception. Sci Rep 12:2760.

1007